Supplementary Information

Noncovalent Assembly of Benzene-Bridged Metallosalphen Dimers: Photoconductive Tapes with Large Carrier Mobility and Spatially Distinctive Conduction Anisotropy

Long Chen, Lu Wang, Xingfa Gao, Shigeru Nagase, Yoshihito Honsho, Akinori Saeki, Shu Seki,* and Donglin Jiang*

Section 1. Materials and Methods

THF was freshly distilled over benzophenone ketyl under Ar before use. Copper acetate monohydrate was obtained from Kanto Chemicals. Benzene-1,2,4,5-tetraamine tetrahydrochloride was obtained from Aldrich. Silica gel Wakogel C–300HG was used for column chromatography. Deuterated solvents for NMR measurement were obtained from Cambridge Isotope Laboratories, Inc. 4-(dodecyloxy)-2-hydroxy-benzaldehyde was prepared according to reported methods.[1]

^{1}H and ^{13}C NMR spectra were recorded on a JEOL model JNM–LA400 NMR spectrometer, where chemical shifts (δ in ppm) were determined with a residual proton of the solvent as standard. Matrix–assisted laser desorption ionization time–of–flight mass (MALDI–TOF MS) spectra were performed on an Applied Biosystems BioSpectrometry

model Voyager–DE–STR spectrometer in reflector or linear mode using 9–nitroanthracene or dithranol as matrix. Elemental analysis was carried out by Atlantic Microlab, Inc. Electronic absorption spectra were recorded using a quartz cell of 1–cm path length on a JASCO model V–570 spectrophotometer equipped with a temperature controller. Infrared (IR) spectra were recorded on a JASCO model FT IR–6100 Fourier transform infrared spectrometer. Field–emission scanning electron microscopy (FE SEM) was performed on a JEOL model JSM–6700 FE–SEM operating at an accelerating voltage of 1.5 or 5.0 kV. Transmission electron microscope (TEM) images were obtained on a JEOL model JEM–3200 microscope. The sample was prepared by drop–casting a THF suspension onto a carbon coated copper grid. AFM images were recorded on a Veeco model 3D multimode diNanoScope with samples deposited on mica. Powder X–ray diffraction (PXRD) data were recorded on a Rigaku model RINT Ultima III diffractometer. Electrochemisty measurements were performed on a BAS Model 610B electrochemical analyzer with a three electrodes configuration, with a cell equipped with a platinum wire as the counter electrode, a platinum disc as the working electrode (2 mm in diameter), and a non aqueous Ag/Ag^+ electrode (Ag wire in 10 mM $AgNO_3$ in anhydrous acetonitrile solution) as the reference electrode. CV measurements were carried out in 0.5 mM freshly distilled THF solution containing 0.1 M tetrabutylammonium hexafluorophophate as electrolyte at a scan rate of 100 mV/s.

Electrical measurements were carried out at ambient temperature in air between a 10-μm-wide Pt electrodes by a two-probe method using a Keithley model 2635 sourcemeter. Typically, a suspension of the tape of **1** in THF (3 μL) was homogenously drop casted onto the electrode to give a film and dried under vacuum. For iodine doping, the tape on electrode was put into an iodine atmosphere for 2h before measurement. For doping with hydrazine, the tape on electrode was put in hydrazine vapor for 2h before measurement. For the sandwich structure device fabrication, a suspension of the tape of **1** in THF (1 mg/mL) was homogenously spin coated (3000 rpm, 25 °C) onto an Al substrate to give a film with thickness around 10 μm and then over coated with 20-nm thick Au. Light irradiation was performed using an Asahi Spectra model MAX-301 Xenon light source, equipped with a heat-cut mirror module. I-V curves were recorded at bias voltages from –2.0 to 2.0 V, on irradiation from the Au electrode with visible light (400 – 700 nm). The film thicknesses were measured by FE SEM.

The laser flash photolysis time-resolved microwave conductivity (FP TRMC) measurements were carried out at 25 °C in Ar or SF_6, where the resonant frequency and microwave power were properly adjusted at 9.1 GHz and 3 mW, respectively. Charge carrier were photochemically generated using the nanosecond laser pulses from a Nd:YAG laser (a third harmonic generation (λ = 355 nm) of Spectra-Physics INDY-HG (FWHM 5 – 8 ns)). The

power density of the laser was set at 3.4 – 14.7 mJ $cm^{-2}pulse^{-1}$. Transient conductivities ($\Phi\Sigma\mu$) were evaluated according to an equation $\Phi\Sigma\mu = (1/A)(\Delta P_r/P_r)$, where A and P_r are sensitivity factor and reflected microwave power, respectively. Time-of-flight transient current integration was measured at 25 °C by photoirradiaiton from with the 355-nm pulse laser. The laser intensity was attenuated at 9.6 mJ $cm^{-2}pulse^{-1}$, while bias voltage was varied from 2 to 16 V. For the fabrication, the tape of **1** was dispersed in toluene (0.2 wt%) and drop-casted onto an Au-interdigitated electrode with 5 μm gap to form a thin film with thickness of about 10 μm.

Section 2. Synthesis and Self-assembly

(1) Synthesis of Benzene–Cored Salphen (**BSH_4**) and Dinuclear Cu(II) Complex (**1**)

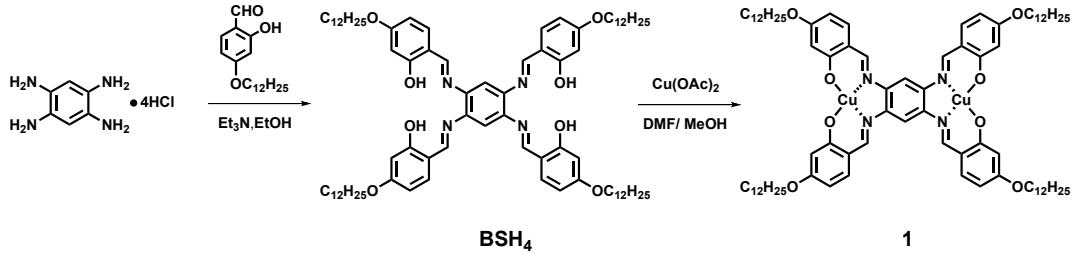

Scheme S1. Synthesis of benzene–cored Schiff base **BSH_4** and dinuclear Cu(II) complex (**1**)[2]

BSH_4: To a suspension of benzene-1,2,4,5-tetramine tetrahydrochloride (0.103 g, 0.36 mmol) in EtOH (4.0 mL) was added Et_3N (0.219 g, 2.16 mmol) under Ar. The mixture was stirred at r.t. for 10 min, added with an EtOH (4.0 mL) solution of 4-dodecyloxy-2-hydroxybenzaldehyde (0.664 g, 2.17 mmol), and the mixture was stirred at reflux for 12 h. The resulting suspension was cooled at –10 °C and stirred for another 1 h. The precipitate was collected by filtration, washed with cold EtOH, and dried under vacuum, to give **BSH_4** (0.361 g, 0.28 mmol) as red solid in 77% yield. ^{1}H NMR (CD_2Cl_2): δ (ppm) 13.47 (s, 4H, O*H*), 8.63 (s, 4H, C*H*=N), 7.31 (d, J = 8.8 Hz, 4H, Ar-*H*), 7.10 (s, 2H, core Ar-*H*), 6.48 (d, J = 2.4 Hz, 4H, Ar-*H*), 6.47 (dd, J = 8.8, 2.4 Hz, 4H, Ar-*H*), 3.99 (t, J = 6.8 Hz, 8H, OCH_2), 1.79 (m, 8H, OCH_2CH_2), 1.28-1.45 (m, 72H, CH_2), 0.88 (t, J = 6.8 Hz, 12H, CH_3). ^{13}C NMR (CD_2Cl_2): δ (ppm) 164.43 (HO-*C*), 164.41 (RO-*C*), 162.46 (*C*H=N), 141.54 (core *C*-N), 134.19, 113.48, 110.10, 108.09, 101.76, 68.79 (OCH_2), 32.32, 30.07, 30.04, 30.01, 29.98, 29.78, 29.75, 29.49, 26.36, 23.08, 14.26 (aliphatic *C*). MALDI–TOF MS for $C_{82}H_{122}N_4O_8$ (Cacld. 1290.93): m/z = 1291.87 ([M + H]$^+$, 100%). UV/Vis (CH_2Cl_2): λ_{max} (nm) (ε / $M^{-1}cm^{-1}$) 289 (3.33×10^4), 360 (6.23×10^4). IR (KBr pellet): ν (cm^{-1}) 2922 (ν_{CH2}), 2852 (ν_{CH2}), 1618 ($\nu_{HC=N}$), 1519, 1235, 1115. Anal. Calcd for $C_{82}H_{122}N_4O_8$: C, 76.24; H, 9.52; N, 4.34. Found: C, 75.80; H, 9.66; N,

4.32%.

1: To a solution of **BSH_4** (0.302 g, 0.23 mmol) in DMF (50 mL) was added a MeOH (5 mL) solution of Cu(II) acetate monohydrate (0.187 g, 0.94 mmol), and the mixture was stirred at 80 °C overnight. The precipitate was collected by filtration and washed with MeOH (10 mL × 3). The resulting solid was dried in vacuum to give **1** (0.288 g, 0.20 mmol) as dark red solid in 87% yield. MALDI–TOF MS for $C_{82}H_{118}Cu_2N_4O_8$ (Cacld. 1414.93): *m*/*z* = 1414.95([M]$^+$, 80%), 1478.19 ([M + Na + K]$^+$, 100%). UV/Vis (CH_2Cl_2): λ_{max} (nm) (ε / $M^{-1}cm^{-1}$) 269 (5.33×10^4), 350 (4.16×10^4), 457 (7.53×10^4), 489 (7.24×10^4), 522 (6.13×10^4). IR (KBr pellet): ν (cm^{-1}) 2919 (ν_{CH2}), 2849 (ν_{CH2}), 1611($\nu_{HC=N}$), 1593, 1506, 1436, 1372, 1319, 1226. Anal. Calcd for $C_{82}H_{118}Cu_2N_4O_8 \cdot H_2O$: C, 68.73; H, 8.44; N, 3.91. Found: C, 69.01; H, 8.50; N, 3.58%.

(2) Synthesis of Controls of Salophen and Mononuclear Cu(II) Complex (**2**)

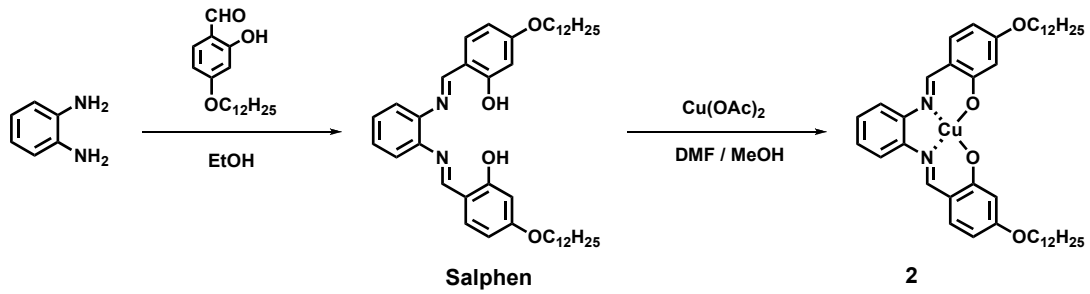

Scheme S2. Synthesis of controls of salophen and mononuclear complex (**2**)

Salphen: To a hot EtOH (1.0 mL) solution of *o*-phenylenediamine (110.8 mg, 1.03 mmol) was added dropwise an EtOH (5.0 mL) solution of 4-dodecyloxy-2-hydroxyl-benzaldehyde (691 mg, 2.25 mmol), and the mixture was stirred at reflux for 12 h. The mixture was cooled at –10 °C, and the resulted yellow precipitate was filtered, washed with cold EtOH, and dried under vacuum, to give **Salphen** (0.525 g, 0.77 mmol) as bright yellow solid in 75% yield. ^{1}H NMR ($CDCl_3$): δ (ppm) 13.58 (s, 2H, O*H*), 8.53 (s, 4H, C*H*=N), 7.30-7.25 (m, 4H, aromatic C*H*), 7.23-7.20 (m, 2H, core aromatic C*H*), 6.52(d, *J* = 2.0 Hz, 2H, aromatic C*H*), 6.46 (dd, *J* = 8.8, 2.0 Hz, 2H, aromatic C*H*), 3.98 (t, *J* = 6.4 Hz, 4H, OCH_2), 1.78 (m, 4H, OCH_2CH_2), 1.27-1.44 (m, 36H, alkyl C*H*), 0.88 (t, *J* = 6.8 Hz, 6H, CH_3). ^{13}C NMR (125.65 MHz, $CDCl_3$): δ (ppm) 164.27 (HO-*C*), 163.72 (RO-*C*), 162.15 (*C*H=N), 142.29 (aromatic *C*-N), 133.47, 127.05, 119.47, 113.04, 109.94, 107.73, 101.65, 68.20 (OCH_2), 31.91, 29.65, 29.62, 29.58, 29.55, 29.34, 29.04, 25.97, 22.69, 14.11 (aliphatic chain *C*). MALDI–TOF MS for $C_{44}H_{64}N_2O_4$ (Cacld. 684.49), *m*/*z* = 685.32 ([M + H]$^+$, 100%). UV/Vis (CH_2Cl_2): λ_{max} (nm) (ε / $M^{-1}cm^{-1}$) 295 (2.47×10^4), 331 (3.06×10^4). IR (KBr): ν (cm^{-1}) 2922 (ν_{CH2}), 2852 (ν_{CH2}), 1610 ($\nu_{HC=N}$), 1583, 1516,

1472. Anal. Calcd. for $C_{44}H_{64}N_2O_4$: C, 77.15; H, 9.42; N, 4.09. Found: C, 76.88; H, 9.43; N, 3.96%.

2: To a suspension of **Salophen** (0.069 g, 0.1 mmol) in DMF (4 mL) was added a MeOH (2 mL) solution of Cu(II) acetate monohydrate (0.04 g, 0.2 mmol) and the mixture was stirred at 80 °C overnight. A greenish brown precipitate was collected by filtration, washed with MeOH (5.0 mL × 3), and evaporated to dryness, to give **2** (0.058 g, 0.077 mmol) as brown solid in 77% yield. MALDI–TOF MS for $C_{44}H_{62}CuN_2O_4$ (Cacld. 745.40), m/z = 768.11 ($[M + Na]^+$, 100%), 784.07 ($[M + K]^+$, 30%). UV/Vis (CH_2Cl_2): λ_{max} (nm) (ε / $M^{-1}cm^{-1}$) 267 (2.51×10^4), 319 (2.57×10^4), 400 (2.87×10^4). IR (KBr): ν (cm^{-1}) 2921 (ν_{CH2}), 2850 (ν_{CH2}), 1617 ($\nu_{HC=N}$), 1578, 1515, 1469, 1436. Anal. Calcd. for $C_{44}H_{62}CuN_2O_4 \cdot H_2O$: C, 68.96; H, 8.42; N, 3.66. Found: C, 68.88; H, 8.35; N, 3.59%.

(3) Self-Assembly

1 (15 mg) was suspended in THF (15 mL) and totally dissolved upon reflux for 30 min. The solution was allowed to cool at 25 °C to give large amount of red orange dark precipitate within 1 hr. The precipitate was collected by centrifugation and dried in vacuum, to give a red orange powder (12.4 mg) in 83% yield.

Section 3. MALDI-TOF MS Spectral Profiles

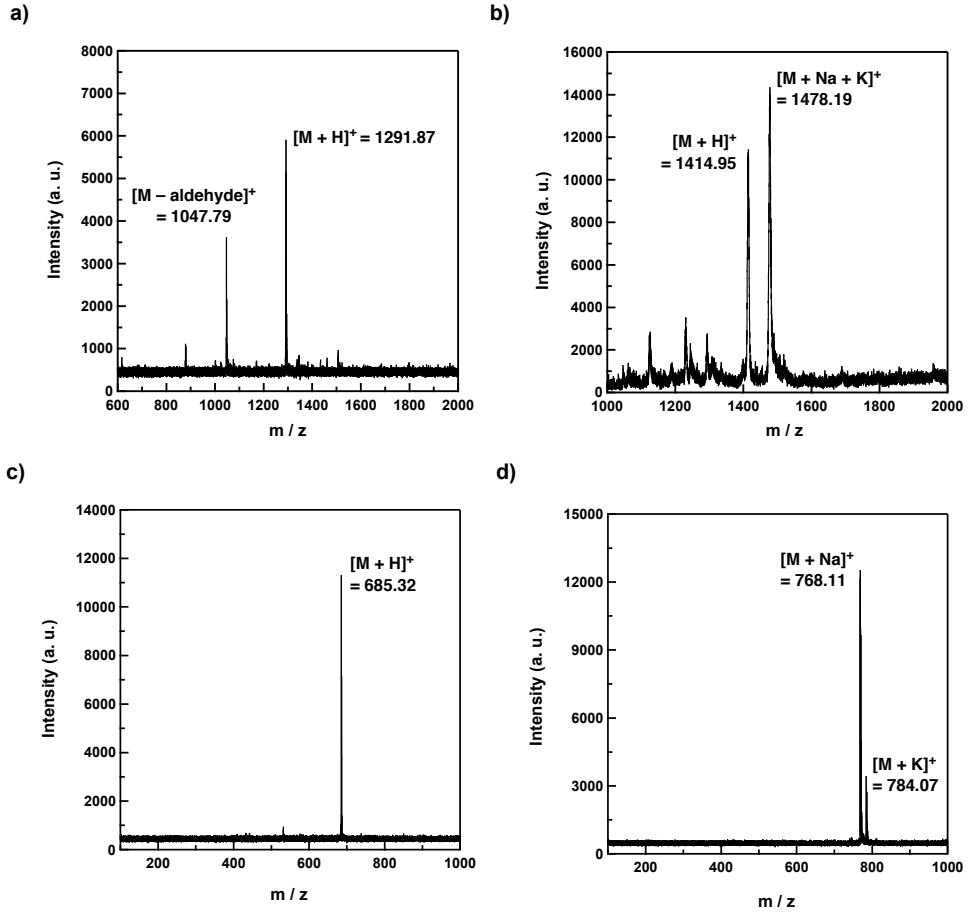

Fig. S1. MALDI–TOF MS spectra. a) **BSH_4**, b) **1**, c) **Salphen**, d) **2**.

Section 4. Cyclic Voltammetric Profile

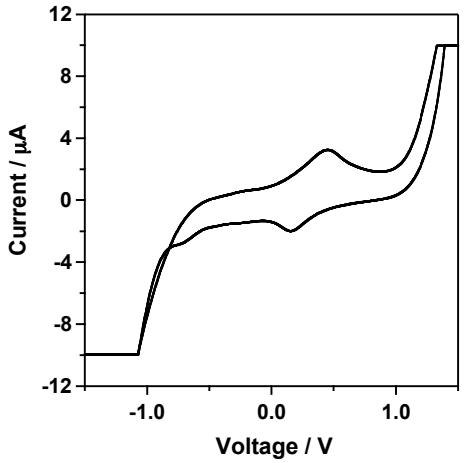

Fig. S2. CV profile of **2** in THF. Only oxidative pair is observable.

Section 5. HOMO-LUMO Gap Calculation

The geometry of the molecule **1** and **2** were fully optimized using the spin-restricted B3LYP/6-31G(d,p) method, which computed the close-shell singlet state for the molecule. To find the ground electronic state, the open-shell singlet and triplet states for **1** and **2** were further studied by calculating the single-point energies using the spin-unrestricted B3LYP/6-31G(d, p) method. The relative energies of the three electronic states (Table 1) show that the triplet state has the lowest energy and is the ground state for **1**. The energy difference between the triplet ground state and the lowest-energy singlet state is 35.7 kcal/mol. The large stability of the triplet state is also reflected by its relatively large energy gaps, the gaps for α- (spin-up) and β-(spin-down) electrons are 2.6 and 2.8 eV, respectively. It is well known that one copper atom possesses a singly occupied *3d* orbital, with a net spin of 1/2. Therefore, the present adoption of triplet as the ground state suggests that the two copper atoms in the molecule only have a weak interaction, which is in good agreement with the large inter-atomic distance calculated for them (7.845 Å). On the other hand, **2** has a doublet ground state; the energy gap of both α- and β-electrons are 3.4 eV. All calculations were performed using the Gaussian 03 program.[3]

Table S1. Relative energies for the three electronic states of **1**.

Electronic State	Relative Energy (kcal/mol)
triplet	0.0
singlet diradical	40.9
close-shell singlet	35.7

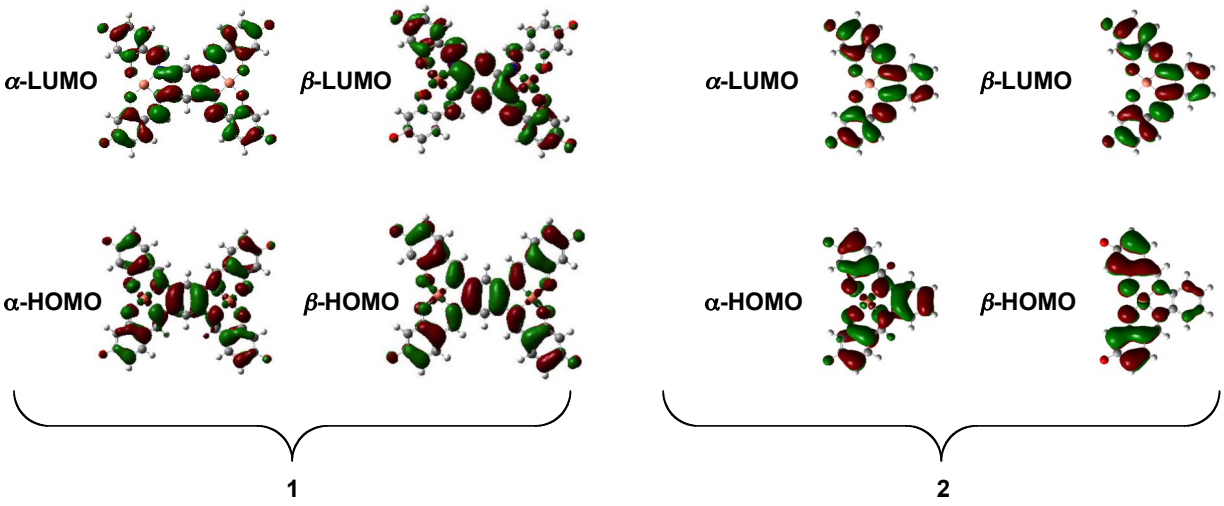

Fig. S3. HOMO-LUMO of **1** and **2** (aliphatic chains are omitted for clarify).

Section 6. Simulation and Calculation of Tape Structure

Powder X-ray diffraction (PXRD) measurement exhibits sharp diffractions at 2θ = 3.83, 5.07, 6.46, 10.28, 15.73, 20.61, and 25.71° (Table S2). Powder X-ray diffraction (PXRD) simulation was carried out by using Reflex, a module implemented in Materials Studio.[4] The lattice parameters of the unit cell were first manually determined from the observed PXRD peaks. Simulated PXRD patterns were calculated and compared with the experimentally observed patterns. The peak broadening was calculated considering the dimensions of the sample (width = 100 nm, length = 1000 nm, thickness = 10 nm). After careful manual refinements, the structure with orthorhombic unit cell (a = 34.76 Å, b = 22.96 Å, c = 6.92 Å) having a staggered AB type arrangement (Chart 1b) shows a good agreement with the experimental PXRD pattern. All the diffraction peaks are reasonably assigned. The *x*-, *y*- and, *Z*-directions in Chart 1b correspond to the width, length, and thickness of the tape, respectively.

Lattice Parameters

a = 34.76 Å, b = 22.96 Å, c = 6.92 Å

$\alpha = \beta = 90°$, $\gamma = 130°$.

Table S2. Simulated and experimentally observed PXRD data.

Simulation					Experiment	
h	k	l	d_{hkl} (Å)	2θ (°)	d (Å)	2θ (°)
1	-1	0	22.95	3.85	23.04	3.83
0	1	0	17.58	5.02	17.41	5.07
2	0	0	13.31	6.64	13.67	6.46
2	-2	0	11.48	7.70	11.31	7.81
0	2	0	8.79	10.06	8.59	10.28
3	-2	1	5.77	15.34	5.63	15.73
3	-4	1	4.37	20.31	4.30	20.61
0	0	2	3.46	25.73	3.46	25.71

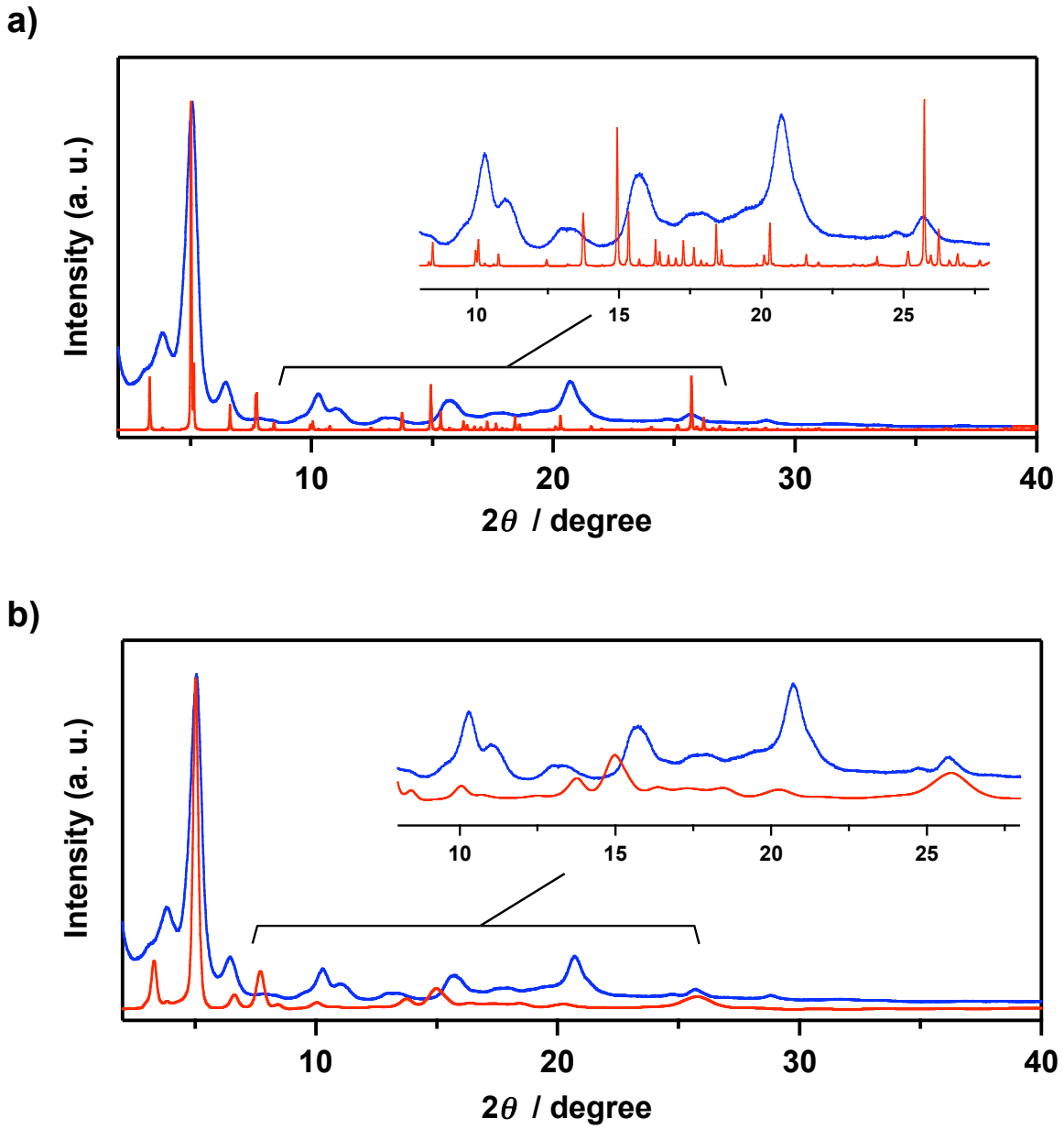

Fig. S4. Experimentally observed (blue curve) and simulated PXRD (red curve) patterns. a) Simulation with the dimensions for the length, width and thickness are infinite, gives very sharp signals in the simulated pattern. b) Simulation with the dimensions for the defined length, width and thickness of the tape (width = 100 nm, length = 1000 nm, thickness = 10 nm) results in broadened simulation pattern. Although the region containing halo scatterings of aliphatic chains (2θ = 10 – 20 °) is difficult to reproduce in both simulations, the positions of important peaks including π-π stack and center–to–center separations are reproduced well in the case of b.

Section 7. FT IR Spectral Profile

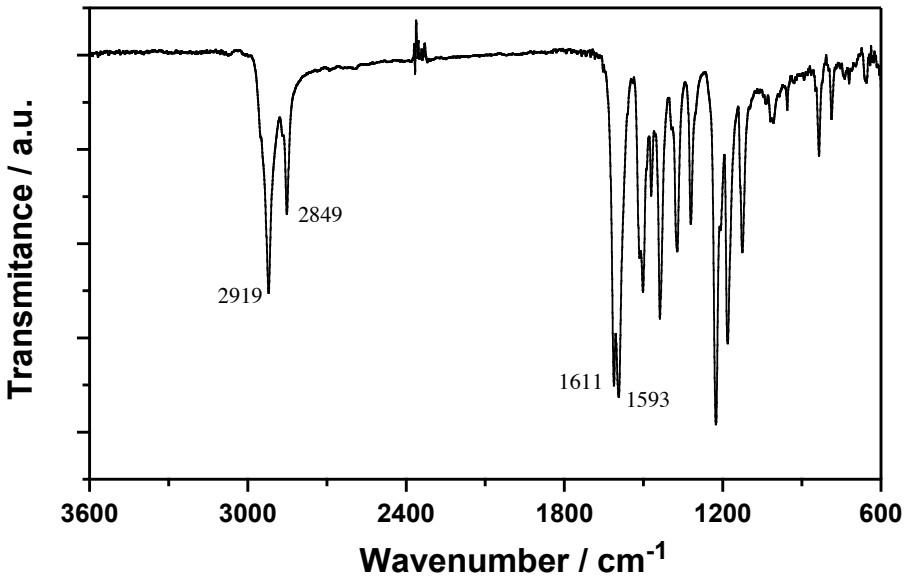

Fig. S5. FT IR spectrum of the tape of **1**.

Section 8. UV-Vis Spectral Change Profiles of Self-assembly Process

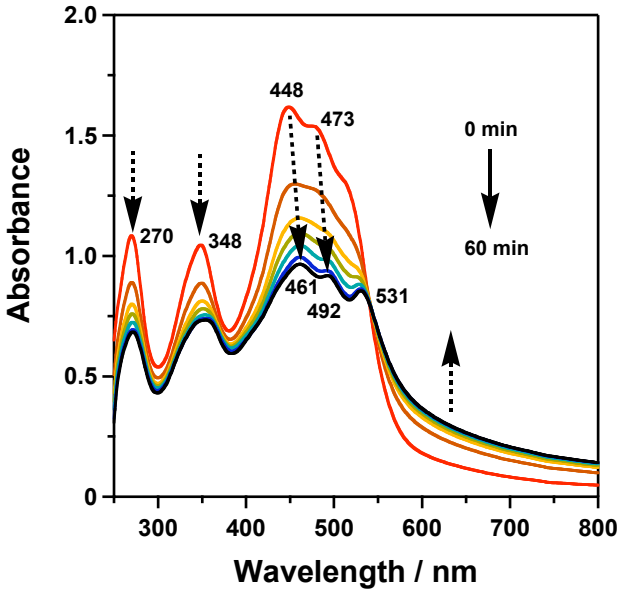

Fig. S6. Time-dependent UV-Vis spectral change profile of **1** in THF. Red shifted peaks observed for self-assembly are typical of the J-type aggregation.

Section 9. On-Off Photocurrent Switching with a 1-μm Thick Film

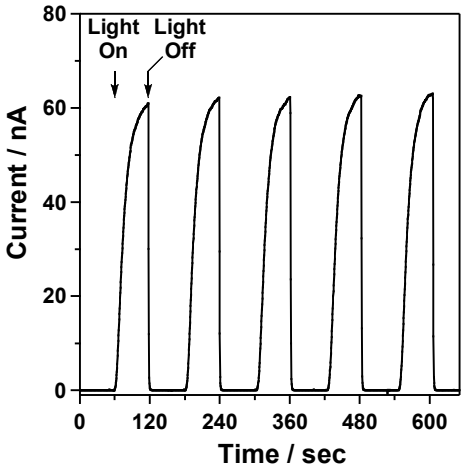

Fig. S7. On-off photocurrent switching with a 1-μm thick film sandwiched between Al/Au electrodes, upon excitation with visible light (400 – 700 nm). The on/off ratio is 4.2×10^5. The switching profile suggests a much abrupt photo-response and high on/off ratio in comparison with the 10-μm thick film.

Section 10. Supporting References

S1) P. Zell, F. Mogele, U. Ziener, B. Rieger, *Chem. Eur. J.,* 2006, **12**, 3847–3857.

S2) A. W. Kleij, M. Kuil, D. M. Tooke, M. Lutz, A. L. Spek, J. N. H. Reek, *Eur. J. Inorg. Chem.,* 2002, 357–368.

S3) Frisch, M. J.; Trucks, G. W.; Schlegel, H. B.; Scuseria, G. E.; Robb, M. A.; Cheeseman, J. R.; Montgomery, J. A.; Vreven, T.; Kudin, K. N.; Burant, J. C.; Millam, J. M.; Iyengar, S. S.; Tomasi, J.; Barone, V.; Mennucci, B.; Cossi, M.; Scalmani, G.; Rega, N.; Petersson, G. A.; Nakatsuji, H.; Hada, M.; Ehara, M.; Toyota, K.; Fukuda, R.; Hasegawa, J.; Ishida, M.; Nakajima, T.; Honda, Y.; Kitao, O.; Nakai, H.; Klene, M.; Li, X.; Knox, J. E.; Hratchian, H. P.; Cross, J. B.; Adamo, C.; Jaramillo, J.; Gomperts, R.; Stratmann, R. E.; Yazyev, O.; Austin, A. J.; Cammi, R.; Pomelli, C.; Ochterski, J. W.; Ayala, P. Y.; Morokuma, K.; Voth, G. A.; Salvador, P.; Dannenberg, J. J.; Zakrzewski, V. G.; Dapprich, S.; Daniels, A. D.; Strain, M. C.; Farkas, O.; Malick, D. K.; Rabuck, A. D.; Raghavachari, K.; Foresman, J. B.; Ortiz, J. V.; Cui, Q.; Baboul, A. G.; Clifford, S.; Cioslowski, J.; Stefanov, B. B.; Liu, G.; Liashenko, A.; Piskorz, P.; Komaromi, L.; Martin, R. L.; Fox, D. J.; Keith, T.; Al-Laham, M. A.; Peng, C. Y.; Nanayakkara, A.; Challacombe, M. P.; Gill, M. W.; Johnson, B. G.; Chen, W.; Wong, M. W.; Gonzalez, C.; Pople, J. A. Gaussian03; Revision C.01 ed.; Gaussian, Inc.: Wallingford CT, 2004.

S4) Accelrys, Material Studio Release Notes, Release 4.4, AccelrysSoftware, San Diego 2009.